J. Fluid Mech. (2006), *vol.* 564, *pp.* 139–158.
doi:10.1017/S0022112006001261 Printed in the United Kingdom

Natural ventilation in interconnected chambers

By M. R. FLYNN[1] AND C. P. CAULFIELD[2,3]

[1]Department of Mechanical and Aerospace Engineering, Jacobs School of Engineering, University of California, San Diego, 9500 Gilman Drive, La Jolla, CA 92093-0411, USA

[2]BP Institute, University of Cambridge, Madingley Rise, Madingley Road, Cambridge, CB3 0EZ, UK

[3]Department of Applied Mathematics and Theoretical Physics, University of Cambridge, Wilberforce Road, Cambridge CB3 0WA, UK

(Received 28 October 2005 and in revised form 27 February 2006)

Ventilation of adjacent, connected chambers, forced in one chamber by an isolated point source of buoyancy is investigated. There are floor- and ceiling-level external openings in the forced and unforced chambers, respectively, while the partition between the chambers has both a floor- and ceiling-level opening. The flow evolves on the time scale over which the volume flux associated with the plume at the ceiling would fill both chambers. The steady state in the forced chamber is analogous to the single chamber flow described by Linden, Lane-Serff & Smeed (*J. Fluid Mech.*, vol. 212, 1990, p. 309), with a well-mixed buoyant upper layer which is deeper than in the single chamber flow due to the extra pressure drop at the upper interior opening. The steady state in the unforced chamber inevitably exhibits vertical stratification, and depends on the transient flow, all the opening areas, and the relative plan area of the two chambers, as is verified by laboratory experiments. When the upper interior opening is relatively large, the buoyant layer in the unforced chamber is deeper than the buoyant layer in the forced chamber, which contradicts model predictions based on the assumption that the layers are always well-mixed.

1. Introduction

Natural ventilation, by which air circulations within buildings are forced by non-mechanical means, is a cost-effective and energy-efficient way of controlling indoor climate in the presence of internal sources of heat. Although the equations that describe buoyant plumes and thermals have been well-known for some time (see for example Morton, Taylor & Turner 1956; Turner 1969; Baines & Turner 1969; Germeles 1975; Manins 1979; List 1982; and Worster & Huppert 1983), it is only within the past two decades that the benefits of applying this knowledge to architectural design have become fully appreciated (see the review of Linden 1999 for details). Most of the studies that have been performed to date consider the ventilation of a single chamber that is connected to the exterior by one or more openings. Analyses have examined both steady-state and transient behaviour of isolated (Linden, Lane-Serff & Smeed 1990, herein referred to as LLS90; Kaye & Hunt 2004) and distributed sources (Gladstone & Woods 2001), as well as the effect of a finite-source volume flux (Caulfield & Woods 2002; Woods, Caulfield & Phillips 2003).

The properties of the final steady state may be determined directly from the source conditions and/or the chamber geometry. Whereas interesting phenomena

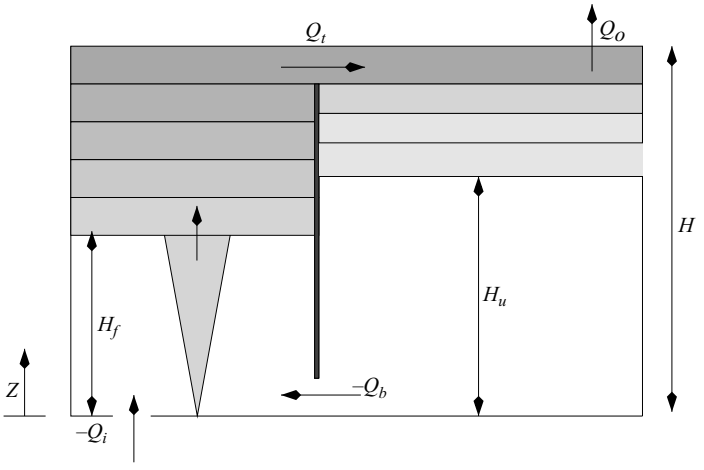

FIGURE 1. Schematic figure of the flow geometry.

may be encountered during the transient flow approach toward steady state (e.g. the 'overshoot' of layer depth remarked upon by Kaye & Hunt 2004), the flow's time history does not affect the steady state.

To demonstrate that this behaviour is not generic, we consider the flow shown schematically in figure 1. There is a single point source of (constant) buoyancy flux F_0 in the left-hand (forced) chamber of depth H, and cross-sectional area A_f. (We follow the convention that upper-case italic letters are used for dimensional quantities.) This chamber has three openings, with in general different effective cross-sectional areas. (For simplicity of exposition, we absorb experimentally determined discharge coefficients into the various opening areas, and assume that the pressure is constant at openings, i.e. they have infinitesimal depth. This ensures unidirectional flow through each opening.) There is one opening (opening '*i*' in the figure) to the exterior at the bottom of the chamber $Z = 0$, with effective cross-sectional area A_i. There are also openings at the bottom ($Z = 0$) and top ($Z = H$) of the chambers (labelled '*b*' and '*t*' in the figure) connecting the left-hand forced chamber to the right-hand (unforced) chamber (of cross-sectional area A_u). These openings in the central partition have effective cross-sectional areas A_b and A_t respectively. Finally, the unforced chamber has an upper opening at $Z = H$ to the exterior (labelled '*o*') with effective cross-sectional area A_o. Although filling-box flows in interconnected chambers have been considered before (see Wong & Griffiths 2001; Lin & Linden 2002) the principal focus has been on the transient dynamics. The flow geometry considered here tends towards a steady state, which nevertheless is determined by the flow's time history.

In § 2, we review the the single chamber model of LLS90, focusing on the aspects of the flow which are particularly relevant to the more general interconnected chamber flow considered here. In § 3, we develop models to describe both the steady-state and transient flows in the interconnected chamber flow, treating separately cases where the buoyant layers in each chamber are assumed to be well-mixed or stratified at intermediate times. In § 4 we discuss the important characteristics of the results of these models, briefly considering some of the implications for real ventilation flows. In § 5 we compare the results of laboratory experiments to our theoretical models, and in § 6 we draw conclusions.

2. Single chamber dynamics

LLS90 considered the flow in a single forced chamber with high- and low-level openings to the exterior (i.e. the flow shown in figure 1 in the absence of the central partition). As the buoyant plume fluid rises to the top of the chamber, a filling box flow is assumed to develop (essentially an assumption on the aspect ratio of the chamber: see Baines & Turner 1969; Hunt, Cooper & Linden 2001 and Conroy, Llewellyn Smith & Caulfield 2005 for more detailed discussion) with a buoyant layer deepening towards the floor. The presence of this buoyant layer leads to the pressure $P_f(H)$ within the chamber at $Z = H$ becoming greater than the pressure in the exterior $P_e(H)$ at that height. This pressure differential drives a flow Q_o through the upper opening, which is given by Bernouilli's equation

$$Q_o = A_o \left[\frac{2}{\rho_e} (P_f(H) - P_e(H)) \right]^{1/2}, \tag{2.1}$$

where ρ_e is the (constant) exterior reference density, and a discharge coefficient has been absorbed into the effective area A_o. This outflow is balanced by an equal and opposite inflow (by convention negative) through the lower opening 'i', i.e.

$$Q_0 + Q_i = 0. \tag{2.2}$$

Assuming that the pressure inside and outside the chamber varies hydrostatically,

$$\frac{P_e(0) - P_f(0)}{\rho_e} = \frac{G}{\rho_e} \int_{H_f}^{H} (\rho_e - \rho_f)\, \mathrm{d}Z - \frac{P_f(H) - P_e(H)}{\rho_e} = \int_{H_f}^{H} G'_f\, \mathrm{d}Z - \frac{P_f(H) - P_e(H)}{\rho_e}, \tag{2.3}$$

where H_f is the interface location of the buoyant layer, $\rho_f(Z, T)$ is the density within this buoyant layer, G is the acceleration due to gravity and G'_f is the reduced gravity of the buoyant fluid in this layer. Using Bernouilli's equation at $Z = 0$, we obtain

$$Q_i = -A_i \left[2 \int_{H_f}^{H} G'_f\, \mathrm{d}Z - \frac{Q_o^2}{A_o^2} \right]^{1/2}, \tag{2.4a}$$

$$\rightarrow -Q_i = Q_o = \frac{A_o A_i}{\left[\frac{1}{2} \left(A_o^2 + A_i^2 \right) \right]^{1/2}} \left(\int_{H_f}^{H} G'_f\, \mathrm{d}Z \right)^{1/2} \equiv A_\star (I_f)^{1/2}, \tag{2.4b}$$

defining the effective opening area parameter $A_\star$ and the buoyancy integral of the forced chamber I_f.

The equation for conservation of mass, under the assumption that diffusive processes are insignificant compared to advective processes, is

$$\frac{\partial}{\partial T} \rho_f = -W_f \frac{\partial}{\partial Z} \rho_f, \tag{2.5}$$

where W_f is the vertical velocity of the buoyant fluid. For the flow to be in steady state, either $\partial \rho_f / \partial Z = 0$, or $W_f = 0$. At steady state, the density is constant everywhere except across a stationary interface at $Z = H_f(t \rightarrow \infty) \equiv H_l$ between a well-mixed buoyant layer and a denser layer of exterior fluid.

In the single chamber flow, the buoyancy integral I_f increases monotonically with time towards a steady-state value, although the location of the interface does overshoot its steady-state value. The depth of the buoyant layer increases due to the 'filling box' flow of plume fluid entering the layer, and decreases due to the

'draining' outflow Q_o. Q_o increases monotonically with I_f, while the plume volume flux decreases monotonically as the depth of the layer increases. Since we assume that the plume fluid spreads instantaneously horizontally with no vertical mixing upon arrival at the ceiling of the chamber, the buoyant layer always exhibits some vertical stratification for $t < \infty$.

The depth of the stratified layer always reaches its steady-state value before I_f has grown to its ultimate steady-state value. This mismatch inevitably leads to an overshoot in the depth of the buoyant layer, as $Q_o < Q_p(H_l)$ at this time. (Kaye & Hunt 2004 discuss the time-dependent behaviour of this system in some detail, under the different simplifying assumption that the buoyant layer is well-mixed for all time, which leads to the different conclusion that the interface location does not always overshoot. Although for flows in single chambers this difference of approach leads to only slight quantitative differences, as we discuss in more detail below, the well-mixed assumption cannot be applied to both interconnected chambers without leading to significant quantitative error.)

As the buoyancy flux F_0 in the plume is constant before its arrival at the interface, the reduced gravity of the plume fluid G'_p at the interface can be simply determined from the classical point-source similarity solution of Zeldovich (1937) and Morton *et al.* (1956):

$$G'_p(Z) = \frac{F_0}{Q_p(Z)} = \frac{F_0}{\lambda F_0^{1/3} Z^{5/3}}, \qquad \lambda = \frac{6\alpha}{5}\left(\frac{9\alpha\pi^2}{10}\right)^{1/3}, \tag{2.6}$$

where α is the (assumed universal) entrainment constant. The requirements of constant steady-state density and volume of the buoyant layer are that $G'_f = G'_p(H_l)$ and $Q_p(H_l) = Q_o$, and so the purely geometric condition defined by LLS90 must hold:

$$\lambda^3 H_l^5 = A_\star^2 (H - H_l). \tag{2.7}$$

Furthermore, the steady state is completely independent of the flow's time history.

3. Interconnected chamber dynamics

For interconnected chambers, as shown in figure 1, (2.2) must still hold. Considering each chamber separately, we obtain

$$Q_b + Q_t = Q_o = -Q_i, \tag{3.1}$$

where Q_b and Q_t are defined as being positive for outflow from the forced chamber.

There is always outflow through opening 'o', inflow through opening 'i', and outflow from the forced chamber through opening 't'. This implies that $P_f(H) > P_u(H) > P_e(H)$ and $P_e(0) > P_f(0)$, and so

$$Q_o = A_o\left[\frac{2}{\rho_e}(P_u(H) - P_e(H))\right]^{1/2}, \qquad Q_t = A_t\left[\frac{2}{\rho_e}(P_f(H) - P_u(H))\right]^{1/2}, \tag{3.2}$$

$$Q_i = -A_i\left[\frac{2}{\rho_e}(P_e(0) - P_f(0))\right]^{1/2}. \tag{3.3}$$

where we have absorbed any discharge coefficients into the effective areas.

Assuming that the pressure distribution is hydrostatic, we obtain

$$\frac{P_e(0) - P_f(0)}{\rho_e} = I_f - \frac{([P_f(H) - P_u(H)] + [P_u(H) - P_e(H)])}{\rho_e}, \tag{3.4}$$

and so

$$\frac{Q_i}{A_i} = -\left(2I_f - \frac{Q_o^2}{A_o^2} - \frac{Q_t^2}{A_t^2}\right)^{1/2} \rightarrow -Q_i = Q_o = A_\star \left(I_f - \frac{Q_t^2}{2A_t^2}\right)^{1/2}. \qquad (3.5)$$

Comparing (2.4) to (3.5), the presence of the unforced chamber, and hence the associated two-stage pressure drop between the forced chamber and the exterior at $Z = H$, manifests itself by a reduction in the ventilation flow through the entire system.

3.1. *Steady-state flow for interconnected chambers*

In steady state, since the depths of both buoyant layers are constant, $Q_b(0) = 0$ and hence $P_f(0) = P_u(0)$. Therefore

$$0 = \frac{2}{\rho_e}[P_f(0) - P_u(0)] = \frac{2}{\rho_e}[P_f(H) - P_u(H)] + 2\int_{H_u}^{H} G'_u \, \mathrm{d}Z - 2I_f, \qquad (3.6a)$$

$$= \frac{Q_t^2}{A_t^2} - 2(I_f - I_u), \qquad (3.6b)$$

where $G'_u = G(\rho_e - \rho_u)/\rho_e$ is the reduced gravity of the buoyant layer in the unforced chamber, and I_u is the related buoyancy integral. Combining this expression with (3.5), we obtain

$$Q_i^2 = Q_t^2 = Q_o^2 = A_\star^2 I_u = \frac{2A_o^2 A_i^2 A_t^2 I_f}{A_o^2 A_i^2 + A_o^2 A_t^2 + A_i^2 A_t^2} = A_\star^2 I_f \left(\frac{2A_t^2}{A_\star^2 + 2A_t^2}\right). \qquad (3.7)$$

At steady state, the properties of the buoyant layer in the forced chamber can be simply determined, and the depth and reduced gravity of this layer are completely independent of the flow's time history. The volume flux out of the buoyant layer in the forced chamber (here Q_t) must be balanced by the volume flux into the layer from the plume, while the density of the (well-mixed) layer in the forced chamber must be balanced by the incoming density of the plume, and so the analogue of (2.7) is

$$\lambda^3 H_{f\infty}^5 = A_\star^2 (H - H_{f\infty}) \left(\frac{2A_t^2}{A_\star^2 + 2A_t^2}\right) = A_\dagger^2 (H - H_{f\infty}), \qquad (3.8)$$

defining a new effective opening area $A_\dagger$ for the interconnected chamber flow. Since $A_\dagger \leqslant A_\star$, the steady-state buoyant layer is always deeper in the interconnected forced chamber than in the single chamber (i.e. $H_{f\infty} < H_l$ where H_l is defined in (2.7)) and hence the ventilation flow Q_o is always less, due to the extra pressure drop across the unforced chamber.

When $A_t \gg A_\star$, $A_\dagger \simeq A_\star$, and so the presence of the partition has little influence on the steady-state flow. Conversely, when $A_t \ll A_\star$, the interface location is completely dominated by the value of A_t, as (3.8) reduces to $\lambda^3 H_{f\infty}^5 \simeq 2A_t^2(H - H_{f\infty})$. This is analogous to the behaviour of the single chamber flow, as noted in LLS90, where if A_i and A_0 are very different in size, $A_\star \simeq \sqrt{2}\min(A_i, A_o)$, and the flow is controlled by the smaller of the two opening areas.

From (3.7), the steady-state flow can also be related to the buoyancy integral I_u for the unforced chamber, in a form identical to the condition (2.4*b*) which pertains in the single chamber flow, since at steady state $P_f(0) = P_u(0)$. Therefore, the pressure difference driving the flow through Q_i is the same as the pressure difference between the exterior and the *unforced* chamber at $Z = 0$. However, everywhere except at the ceiling of the unforced chamber, where since $Q_t = Q_o$ the buoyant fluid entering

the unforced chamber immediately leaves, the steady-state flow is stationary in the unforced chamber, and so the properties of the unforced layer cannot be determined without considering the complete flow history. Indeed, since the buoyant layer develops transiently due to more buoyant fluid flowing into the unforced chamber (through opening 't' from the forced chamber) than is driven out to the exterior through opening 'o' to the exterior, the buoyant layer in the unforced chamber must be vertically stratified in a way determined by the transient evolution.

3.2. *Transient flow dynamics for interconnected chambers*

As we discuss in Appendix A, it is possible to establish that $Q_b \leqslant 0$, and so there is never any flow through opening 'b' from the forced chamber into the unforced chamber, if the buoyant layer in the unforced chamber is assumed to be stratified. Therefore,

$$Q_b = -A_b \left(\frac{2}{\rho_e} [P_u(0) - P_f(0)] \right)^{1/2} = -A_b \left[2(I_f - I_u) - \frac{Q_t^2}{A_t^2} \right]^{1/2}, \tag{3.9}$$

using (3.2), closing the transient system. It is convenient for the subsequent analysis to non-dimensionalize the flow quantities.

From the properties of the steady state, $A_\star$ still figures prominently, and so we use $A_\star$ to scale the two interior opening areas

$$a_t = \frac{A_t}{A_\star}, \qquad a_b = \frac{A_b}{A_\star}, \qquad a_\dagger = \frac{A_\dagger}{A_\star} = \left(\frac{2a_t^2}{1 + 2a_t^2} \right)^{1/2}. \tag{3.10}$$

(We follow the convention that lower-case italic letters are used for non-dimensional quantities.) Volume fluxes are non-dimensionalized with the volume flux Q_H which a point-source plume with buoyancy flux F_0 satisfying the similarity solution (2.6) would have at the ceiling, i.e.

$$q_o = \frac{Q_o}{Q_H}, \qquad q_i = \frac{Q_i}{Q_H}, \qquad q_t = \frac{Q_t}{Q_H}, \qquad q_b = \frac{Q_b}{Q_H}, \qquad Q_H = \lambda F_0^{1/3} H^{5/3}. \tag{3.11}$$

The natural time scale for the flow is the filling-box time scale for the two chamber system, defined here as

$$T_f = \frac{(A_f + A_u)H}{Q_H}, \tag{3.12}$$

i.e. the time that a source with volume flux Q_H would take to fill both chambers (with total cross-sectional area $A_f + A_u$). The relative volume of the two chambers plays a critical role in the time-dependent behaviour of the system, and so we define the non-dimensional quantity $a_u = A_u/A_f$. We also scale vertical distances with the depth H, i.e. $z = Z/H$, $h_f = H_f/H$, $h_u = H_u/H$, $h_{f\infty} = H_{f\infty}/H$, and $h_l = H_l/H$.

We choose to use H and $G'_H = F_0/Q_H$, the reduced gravity at the ceiling of a point-source plume with buoyancy flux F_0 to scale the buoyancy integrals, i.e.

$$i_u = \frac{I_u}{G'_H H} = \frac{\lambda H^{2/3} I_u}{F_0^{2/3}}, \qquad i_f = \frac{\lambda H^{2/3} I_f}{F_0^{2/3}}. \tag{3.13}$$

Therefore, at steady state

$$i_u = a_\dagger^2 i_f, \tag{3.14}$$

while, in general

$$q_o + q_i = 0, \qquad q_b + q_t = q_o, \qquad 2q_o^2 + \frac{q_t^2}{a_t^2} = \frac{2i_f}{\mu^2}, \tag{3.15}$$

where μ is the non-dimensional opening area parameter (or equivalently time scale ratio) as defined in Kaye & Hunt (2004), i.e.

$$\mu^2 = \frac{\lambda^3 H^4}{A_\star^2} = \frac{T_d^2}{T_f^2}. \tag{3.16}$$

The draining time scale T_d is defined as

$$T_d = \frac{(A_f + A_u)H}{A_\star (G'_H H^{1/2})}. \tag{3.17}$$

This is the characteristic time scale for buoyant fluid with this reduced gravity to drain from the two chambers, in the absence of the internal partition. (See Kaye & Hunt 2004 for a more detailed discussion.)

Non-dimensionalizing (3.9), we obtain

$$\frac{q_b^2}{a_b^2} = \frac{2(i_f - i_u)}{\mu^2} - \frac{q_t^2}{a_t^2}. \tag{3.18}$$

Combining this equation with (3.15), it is apparent that, provided $q_o \leqslant q_t$,

$$i_u \leqslant \mu^2 q_o^2 \leqslant a_\dagger^2 i_f, \tag{3.19}$$

and so $a_\dagger^2 i_f - i_u \geqslant 0$, and i_u approaches its steady state value from below for circumstances where the buoyant layer in the unforced chamber is assumed to remain stratified, since as discussed in Appendix A, the flow through opening 'b' is unidirectional.

Using (3.15) and (3.18), to eliminate q_b and q_t, q_o^2 must satisfy a quadratic equation. Requiring that q_o converges towards its steady-state value $q_o \to \sqrt{i_u}/\mu$, we obtain

$$q_o^2 = \frac{i_u}{\mu^2} + \frac{4a_b^2 i_u + \left[1 + 2\left(a_t^2 + a_b^2\right)\right]\left[1 + 2a_t^2\right]\left[a_\dagger^2 i_f - i_u\right]}{\mu^2\left[1 - 4\left(a_b^2 - a_t^2\right) + 4\left(a_b^2 + a_t^2\right)^2\right]} - \frac{\left[16a_b^4 i_u^2 + 16a_b^2\left(1 + 2a_t^2\right)\left(a_\dagger^2 i_f - i_u\right)\left(a_b^2 i_u + a_t^2 i_f\right)\right]^{1/2}}{\mu^2\left[1 - 4\left(a_b^2 - a_t^2\right) + 4\left(a_b^2 + a_t^2\right)^2\right]}. \tag{3.20}$$

All the other volume fluxes can be determined from (3.15).

We assume that the plume is rising from a 'point' source of buoyancy flux alone. We also assume that the plume is sufficiently narrow that it may be modelled as isolated, and that, at all heights within the plume $\pi B^2 \ll A_f$, where B is the plume radius. This conventional assumption (see Conroy *et al.* 2005 for a detailed discussion) also ensures that the aspect ratio of the chamber is sufficiently small for a quasi-steady approximation to be made, so the plume rising through the chamber may be treated as flowing through a time-independent ambient, which in turn evolves on a very much slower time scale.

Also, as mentioned in the Introduction, we assume that the aspect ratio is sufficiently small that a 'filling box' flow can develop, with the plume fluid arriving at the top of the chamber and spreading to form a buoyant layer (thus leading to stratification in the chamber) rather than driving an overturning, mixing the fluid in the entire chamber. Finally, we assume that the flow is at sufficiently high Reynolds numbers

that advective processes dominate diffusive processes. We make a similar assumption in the unforced chamber, so that flow through opening 't' is not fast enough to overturn the buoyant layer in the unforced chamber. Nevertheless, for solving the transient problem, four different possibilities exist, since the buoyant layer in each chamber can be modelled as either well-mixed or continuously stratified.

3.2.1. *Stratified buoyant layer in the forced chamber*

In the forced chamber, using the non-dimensionalization chosen, the plume equations are

$$\frac{\partial}{\partial z}q = \frac{5}{3}m^{1/2}, \qquad \frac{\partial}{\partial z}m = \frac{4fq}{3m}, \qquad \frac{\partial}{\partial z}f = -q\frac{\partial}{\partial z}g'_f, \tag{3.21a–c}$$

where

$$q = \frac{Q}{Q_H}, \qquad M = \frac{M}{M_H} = \frac{M}{\left(\frac{9}{10}\alpha\pi^2 F_0 H^2\right)^{2/3}}, \qquad f = \frac{F}{F_0}, \qquad g'_f = \frac{G'_f}{G'_H}, \tag{3.22}$$

and the boundary conditions are $q(0) = 0 = m(0)$, $f(0) = 1$. The system is closed by considering the equation for conservation of mass (2.5) at all heights in the forced chamber. Under the above assumptions, the return velocity W_f of ambient fluid in the forced chamber is $-(Q - Q_t)/A_f$, as there is a net flow of Q_t through the chamber. Therefore, g'_f satisfies

$$\frac{\partial}{\partial t}g'_f = -(q - q_t)(1 + a_u)\frac{\partial}{\partial z}g'_f, \tag{3.23}$$

with initial condition $g'_f(z) = 0$.

Equations (3.21) and (3.23) can be solved using the method of Germeles (1975), who developed a numerical model for single chamber flow to solve (3.21) and (3.23). The plume equations are integrated through the ambient chamber stratification, modelled by a sufficiently large number of discrete layers, separated by interfaces. The location of each interface is then updated using (3.23). At every time step, a new layer is added at the ceiling of the chamber, with reduced gravity $g'_p(1)$ given by the reduced gravity of the arriving plume fluid, which is assumed to spread out instantly without any mixing. This model can be straightforwardly generalized to the interconnected chamber case by tracking correctly the volume flux q_t and the reduced gravity of fluid which leaves through opening 't' at any time instant. Using (3.15) and (3.20), q_t can be determined provided i_u and i_f are determined. The integrals i_f and i_u are calculated directly from the chambers' reduced gravity distribution.

3.2.2. *Well-mixed buoyant layer in the forced chamber*

As noted by Baines & Turner (1969), and discussed by Worster & Huppert (1983), the density stratification which develops typically has a weak variation through much of the buoyant layer, with a region of strong variation near the base. Also, as noted by Kaye & Hunt (2004), in laboratory experiments, there is inevitably some mixing as the plume fluid spreads at the ceiling of the chamber. It is appealing to assume that the layer is well-mixed (mimicking the steady state) and so only the interface location h_f and the well-mixed layer reduced gravity g'_f need to be modelled. We obtain

$$\frac{\mathrm{d}}{\mathrm{d}t}h_f = (1 + a_u)\left(q_t - h_f^{5/3}\right), \qquad \frac{\mathrm{d}}{\mathrm{d}t}g'_f = \frac{(1 + a_u)\left(1 - g'_f h_f^{5/3}\right)}{1 - h_f}. \tag{3.24}$$

These coupled equations then can be used to describe the evolution of the buoyant layer in the forced chamber, once again provided q_t can be identified, and hence provided i_u is known, as in this case, there is the simple relationship $i_f = g'_f(1-h_f)$.

3.2.3. *Stratified buoyant layer in the unforced chamber*

Since the unforced chamber is supplied horizontally through opening 't', the likelihood of substantial overturning within the chamber as the buoyant layer develops is not as significant as in the forced chamber, and the steady state is not necessarily well-mixed. As already noted $q_o \leqslant q_t$ at all times, and so the buoyant layer is continually supplied by incoming fluid from the forced chamber through opening 't', of reduced gravity $g'_t = g'_p(1)$ if the forced chamber is assumed to be stratified, or $g'_t = g'_f$ if it is assumed to be well-mixed. If we assume that there is no mixing in the unforced chamber, the net volume flux of $q_t - q_o$ spreads out layer by layer, developing a vertical stratification in the unforced chamber. The depth of this layer, and the value of the integral i_u can be calculated by tracking all these incoming layers, which descend at the same non-dimensional speed $(q_o - q_t)(1+a_u)/a_u$ in the unforced chamber.

3.2.4. *Well-mixed buoyant layer in the unforced chamber*

Of course, if it is assumed that the fluid in the unforced chamber is well-mixed, it can be characterized by a single reduced gravity g'_u and the interface location h_u. The equations for the evolution of these quantities then take the form

$$\frac{\mathrm{d}}{\mathrm{d}t}h_u = \frac{(q_t - q_o)(1+a_u)}{a_u}, \qquad \frac{\mathrm{d}}{\mathrm{d}t}g'_u = \frac{(g'_t - g'_u)(1+a_u)q_t}{a_u(1-h_u)}, \tag{3.25}$$

where g'_t is the reduced gravity of the fluid entering through opening 't'. This last equation is particularly interesting, as it does not involve the flow through opening 'o' at all. Indeed, as we discuss in Appendix B, for this well-mixed model it is possible for the flow to reverse direction through opening 'b', and hence for the interface location h_u in the unforced room to overshoot its final position. The steady state associated with this well-mixed model occurs when $q_t = q_o$, and hence the two interfaces are stationary. However, (3.25) implies that at steady state $g'_f = g'_u$. Therefore, from (3.7), at steady state,

$$g'_u(1-h_u) = a_\dagger^2 g'_f(1-h_f) \rightarrow (1-h_u) = \frac{2a_t^2}{1+2a_t^2}(1-h_f), \tag{3.26}$$

and so the buoyant layer depth in the unforced chamber is predicted to be always less than the buoyant layer depth in the forced chamber.

We are not aware of a careful analysis of the dependence of the predictions of transient models on mixing assumptions within developing layers, even in the single chamber case. Here we will compare the results of the two extreme situations, i.e. we will assume that both chambers remain stratified (which we will refer to as the S-S model, denoting stratification in both chambers) or that both may be modelled with well-mixed buoyant layers (referred to as the M-M model, denoting well-mixed models in both chambers).

There is still a very large parameter space which could be considered. We choose a single value of $\mu = 4$, which corresponds to a steady-state interface for the single chamber flow at the midpoint $h_l = 1/2$ of the chamber. This choice avoids extreme values for the buoyant layer depth in the forced chamber of the interconnected chamber flow. We are considering a situation where the draining time scale T_d (3.17)

is larger than the filling-box time scale T_f (3.12) but of the same order. To identify the influence of the other parameters, we consider eight different situations in detail, with essentially 'large' and 'small' values for each of the three areas a_t, a_b and a_u. We are particularly interested in the extent to which the reduced well-mixed M-M model agrees with the more detailed stratified S-S model.

We have chosen the parameters deliberately to avoid certain complicated flow regimes, which though potentially interesting, are beyond the scope of the present study. For example, if the opening areas are chosen to be sufficiently small, so that $H_{f\infty}$ (as defined in (3.8)) is sufficiently close to zero, exchange flow of buoyant fluid may occur at opening 'b' between the two chambers. A similar phenomenon may occur (particularly when the unforced chamber is sufficiently narrow compared to the forced chamber, and $H_{f\infty}$ is sufficiently small) with the buoyant layer flowing from unforced chamber into the forced chamber, thus leading to a recycling of buoyant fluid (a phenomenon related to some of the flows considered in Wong & Griffiths 2001). It is straightforward to identify the parameter regimes where these phenomena are predicted to occur, and we intend to report on the behaviour of the flow system under those circumstances in the future.

4. Model results

We consider the eight different combinations of $a_u = 1/2$ and 2 (corresponding to our experimental situation), a_t^2, $a_b^2 = 1/10$, and a_t^2, $a_b^2 = 10$. In figures 2–4, we compare the important mean flow quantities predicted by the M-M and the S-S models for the various flow geometries: the flow rates q_t and q_o out of the forced chamber and unforced chamber; the buoyant layer depths h_f and h_u; and the mean (or well-mixed) reduced gravities, which for the S-S model, are defined as

$$\overline{g'_f} = \frac{i_f}{1-h_f}, \qquad \overline{g'_u} = \frac{i_u}{1-h_u}. \tag{4.1}$$

As shown in figure 2, in general there is a quite close agreement between the flow rates predicted by the well-mixed M-M model and the stratified S-S model, implying that the predicted values of i_f and i_u also agree closely. From (3.7), increasing a_t increases the steady-state value of the flow rate through the system. Perhaps most interestingly, increasing a_t and especially a_b leads to significant transient increase in q_t, which is substantially larger than q_o, particularly when the forced room is relatively small compared to the unforced room (and hence a_u is large). This transient response is due to the combination of two effects: the relatively rapid deepening of the buoyant layer in the forced room, and the large cross-sectional area of the internal openings allowing substantial flow from the forced room to the unforced room. For the well-mixed M-M model, typically $q_t < q_o$ eventually, so (B 3) is used to determine the flow rates, and the M-M model predicts overshoot of the unforced layer interface, although this overshoot is quite small.

As is apparent in figures 3 and 4, for the forced chamber, the well-mixed M-M model also agrees closely with the stratified S-S model, as the plume dynamics rapidly lead to the density distribution in the forced chamber being well-mixed. The interface location in the forced chamber also exhibits overshoot, and typically converges to a value somewhat less than that predicted for a single chamber flow ($h_l = 1/2$). When the interconnecting openings are relatively large, and so flow between the two chambers is relatively large, the reduction in the steady-state interface height is relatively small. However decreasing a_t can reduce the interface height substantially,

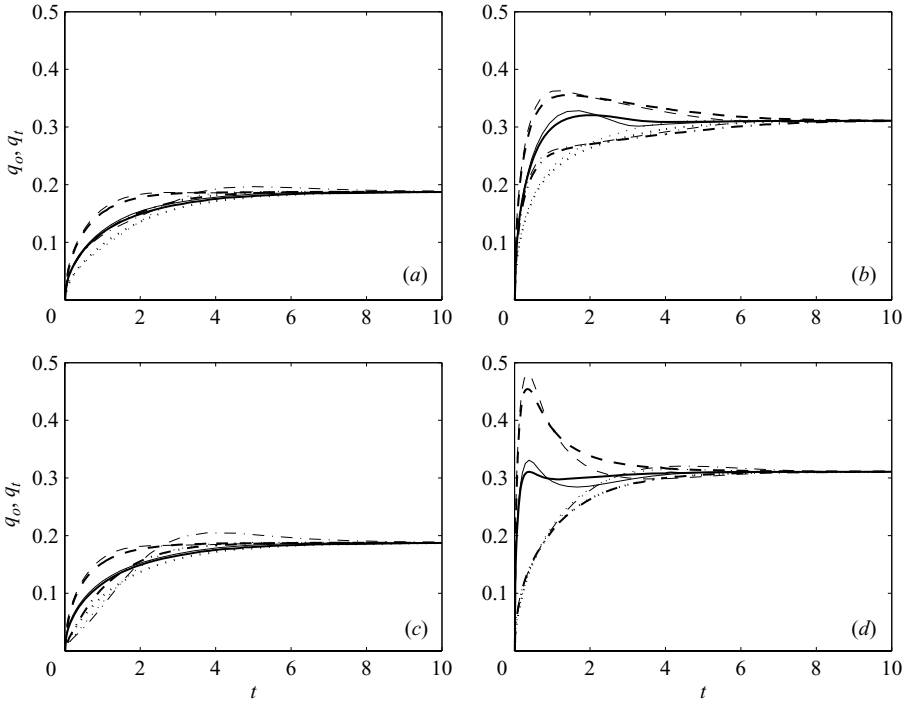

FIGURE 2. Plots against time of q_t (plotted with a solid line for systems with $a_u = 1/2$, and with a dashed line for $a_u = 2$) and q_o (dotted line for $a_u = 1/2$ and dot-dashed line for $a_u = 2$) as predicted by the stratified S-S model (thick lines) and reduced M-M model (thin lines) for systems with $h_l = 1/2$ and: (*a*) $a_t^2 = 0.1$, $a_b^2 = 0.1$; (*b*) $a_t^2 = 10$, $a_b^2 = 0.1$; (*c*) $a_t^2 = 0.1$, $a_b^2 = 10$; (*d*) $a_t^2 = 10$, $a_b^2 = 10$.

as in this case the controlling opening area $A_\dagger \sim A_t$ in (3.8). This reduction in turn increases the steady-state value of $\overline{g'_f}$ substantially.

When a_t^2 is small, the system with a relatively small forced-chamber cross-sectional area (i.e. a_u large, plotted with dashed lines) exhibits slightly more rapid deepening and rapid increase in $\overline{g'_f}$ than the system with smaller a_u (plotted with solid lines). This is due to the restriction of flow through opening 't' leading to a disproportionate amount of buoyant fluid remaining in the forced chamber, which leads both to rapid deepening and more rapid increase in reduced gravity. The area of the lower 'b' opening also has an effect on the speed of convergence of the forced layer to its steady-state value, particularly when a_t is large, although there is no effect of either a_u or a_b on the ultimate steady state in the forced chamber. As is apparent in figures 2(*b*) and 2(*d*), smaller a_b corresponds to a smaller peak value of q_t, as the communication between the two chambers is somewhat suppressed.

There are significant differences between the predictions of the two models for the properties of the flow in the unforced chamber. For the stratified S-S model, there is strong dependence of the ultimate steady states on all of the area parameters: a_t, a_b and a_u. In general, increasing a_u increases the steady-state values of h_u and $\overline{g'_u}$ in such a way that the steady-state value of $i_u = \overline{g'_u}(1-h_u)$ is constant. When a_u is larger, the buoyant layer tends to be shallower in the unforced chamber, and so the steady-state reduced gravity is somewhat larger. The relative change in $\overline{g'_u}$ is largest when a_b and

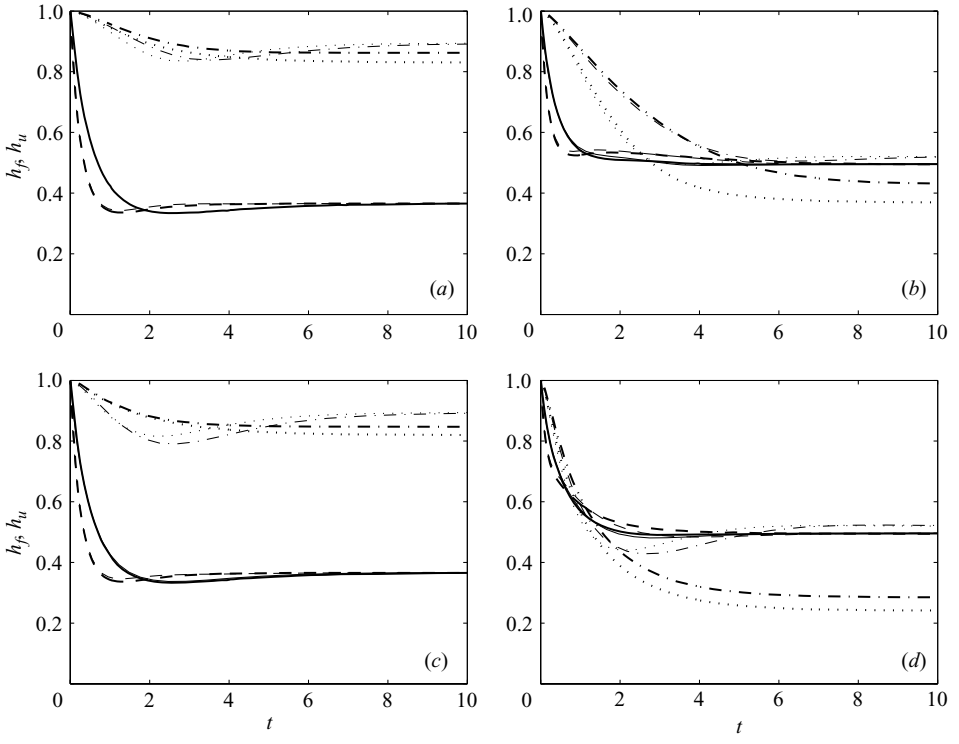

FIGURE 3. Plots against time of the forced chamber interface location h_f (plotted with a solid line for systems with $a_u = 1/2$, and with a dashed line for $a_u = 2$) and the unforced chamber interface location h_u (dotted line for $a_u = 1/2$ and dot-dashed line for $a_u = 2$) as predicted by the stratified S-S model (thick lines) and reduced M-M model (thin lines) for systems with $h_l = 1/2$ and: (*a*) $a_t^2 = 0.1$, $a_b^2 = 0.1$; (*b*) $a_t^2 = 10$, $a_b^2 = 0.1$; (*c*) $a_t^2 = 0.1$, $a_b^2 = 10$; (*d*) $a_t^2 = 10$, $a_b^2 = 10$.

in particular a_t is small, as that corresponds to small values of the unforced chamber's buoyant layer depth $1 - h_u$, which exhibits large relative changes with a_u.

Although increasing a_b tends to decrease both interface height and reduced gravity at steady state, by far the strongest effects are associated with variations in a_t. Increasing a_t, and thus allowing for increased volume flow between the two chambers even at steady state, leads inevitably to a significant increase in the depth of the unforced buoyant layer. This deeper layer typically also has a smaller reduced gravity. Relatively more of its volume comes from the early, transient, peak of volume flow through the upper opening, which has low reduced gravity since it comes from plume fluid which has been diluted through entrainment by ambient fluid through virtually all of its rise.

Furthermore, typically, the mean reduced gravity is eventually lower in the unforced chamber than in the forced chamber, because the buoyant layer in the unforced chamber always contains fluid of relatively low reduced gravity from early in the flow evolution, when the plume has been strongly diluted. Essentially, the stratified S-S model predicts widely varying relative depths of the two buoyant layers. Small values of a_t (and thus little flow between the two chambers at early times) implies that $h_u > h_f$, (figure 3*a*) while larger values of a_t (and to a lesser extent a_b) and hence larger flow rates q_t imply substantially smaller values of h_u (figure 3*d*).

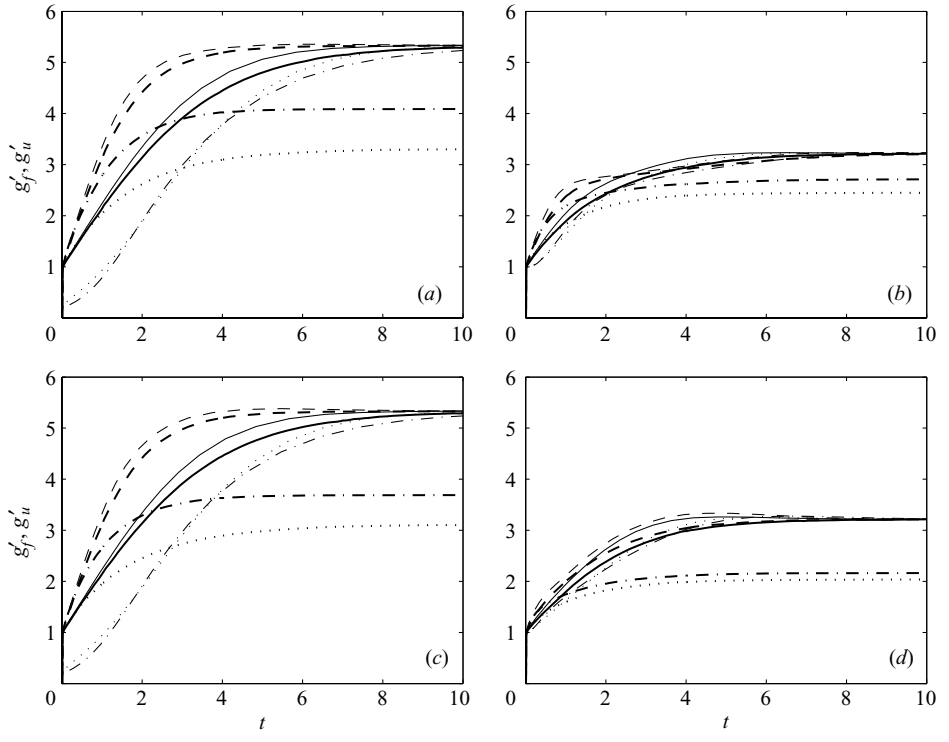

FIGURE 4. Plots against time of the mean or well-mixed forced chamber reduced gravity $\overline{g'_f}$ (plotted with a solid line for systems with $a_u = 1/2$, and with a dashed line for $a_u = 2$) and the mean or well-mixed unforced chamber reduced gravity $\overline{g'_u}$ (dotted line for $a_u = 1/2$ and dot-dashed line for $a_u = 2$) as predicted by the stratified S-S model (thick lines) and reduced M-M model (thin lines) for systems with $h_l = 1/2$ and: (*a*) $a_t^2 = 0.1$, $a_b^2 = 0.1$; (*b*) $a_t^2 = 10$, $a_b^2 = 0.1$; (*c*) $a_t^2 = 0.1$, $a_b^2 = 10$; (*d*) $a_t^2 = 10$, $a_b^2 = 10$.

The predictions of the well-mixed M-M model are qualitatively different. The reduced gravity of the unforced layer always converges to that of the forced layer. This forces the interface location to be given by the simple formula (3.26), predicting that $h_u > h_f$ in all cases, which is qualitatively different from the S-S model, as shown in figure 3. The M-M model predicts overshoot in the unforced layer's interface location in all cases, and a little variation in h_u with the parameter a_u. Figure 4 shows that the predictions for $\overline{g'_u}$ also depend weakly on a_u. For smaller values of a_t, convergence to g'_f is somewhat slower, due to the restriction of flow between the two chambers.

For the S-S model, we also plot the evolution of the vertical profiles of reduced gravity g'_f and g'_u in figures 5 and 6 respectively at $t = n/2$, $n = 1, 2, \ldots, 20$, for systems with $a_u = 1/2$, $h_l = 1/2$, and the four previously used choices of a_t and a_b. (The interfaces move downwards slightly more rapidly in the forced chamber and conversely more slowly in the unforced chamber when $a_u = 2$, as in each case the downwards propagation is relatively faster in the relatively smaller chamber.) The evolution of the reduced gravity profile in the forced chamber is very similar to the emptying filling box behaviour in a single chamber previously considered in LLS90. Quite rapidly, the buoyant layer becomes essentially well-mixed, and there is very little vertical variation in density, and hence little impact on q_t, h_f and $\overline{g'_f}$, and so it is unsurprising that the predictions of the two models agree closely.

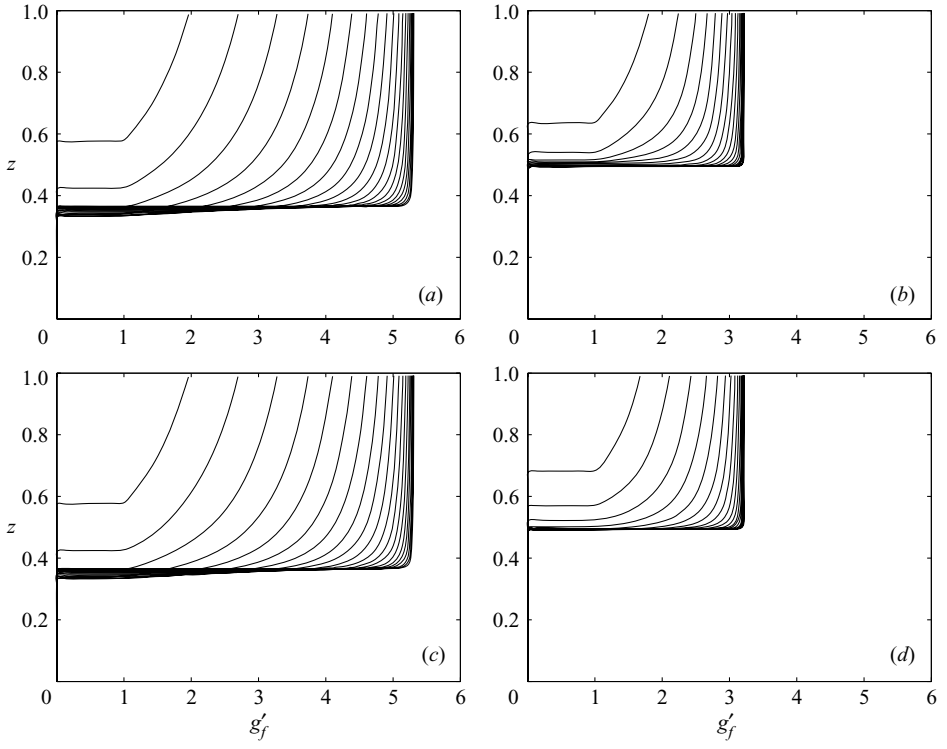

FIGURE 5. Profiles of $g'_f(z)$ predicted by the stratified S-S model at times $t = n/2$, $n = 1, 2, \ldots, 20$, for systems with $a_u = 1/2$, $h_l = 1/2$, and: (*a*) $a_t^2 = 0.1$, $a_b^2 = 0.1$; (*b*) $a_t^2 = 10$, $a_b^2 = 0.1$; (*c*) $a_t^2 = 0.1$, $a_b^2 = 10$; (*d*) $a_t^2 = 10$, $a_b^2 = 10$.

The predictions are markedly different for the profiles of g'_u in the unforced chamber. When a_t is small, the steady-state buoyant layer in the unforced chamber is relatively shallow, while the steady-state value of $\overline{g'_f}$ is relatively large. Therefore small quantities of fluid with relatively rapidly varying reduced gravity are deposited in the unforced chamber. This variation leads to a strongly stratified final steady state in the unforced chamber. At steady state the unforced chamber has no vertical motion (unlike the forced chamber) and so non-zero values of $\partial\rho/\partial z$ are not inconsistent with $\partial\rho/\partial t = 0$ in (2.5). Indeed, although their structure is somewhat more complicated for larger values of a_t and a_b (associated with the non-trivial variation with time of the flow rates through the openings), all the profiles of g'_u appear to exhibit strong vertical stratification for all times.

The time scale of convergence towards steady state is the filling-box time scale T_f for the two chamber system as defined in (3.12). Therefore, in circumstances where the cross-sectional area of the unforced chamber is substantially larger than that of the forced chamber (i.e. $A_f \ll A_u$ as defined in the description of figure 1) the approach to steady state of the forced chamber is substantially delayed by the presence of the large, yet finite unforced chamber. This phenomenon of delayed convergence may have relevance in real buildings, where smaller chambers (e.g. offices, shops) are connected to larger atria. The character of the steady state in the unforced chamber is typically stratified, and depends strongly on the time-dependent evolution of the flow. Particularly when the upper opening 't' is relatively large, the unforced chamber's buoyant layer is deeper at steady state than the buoyant layer in the forced chamber.

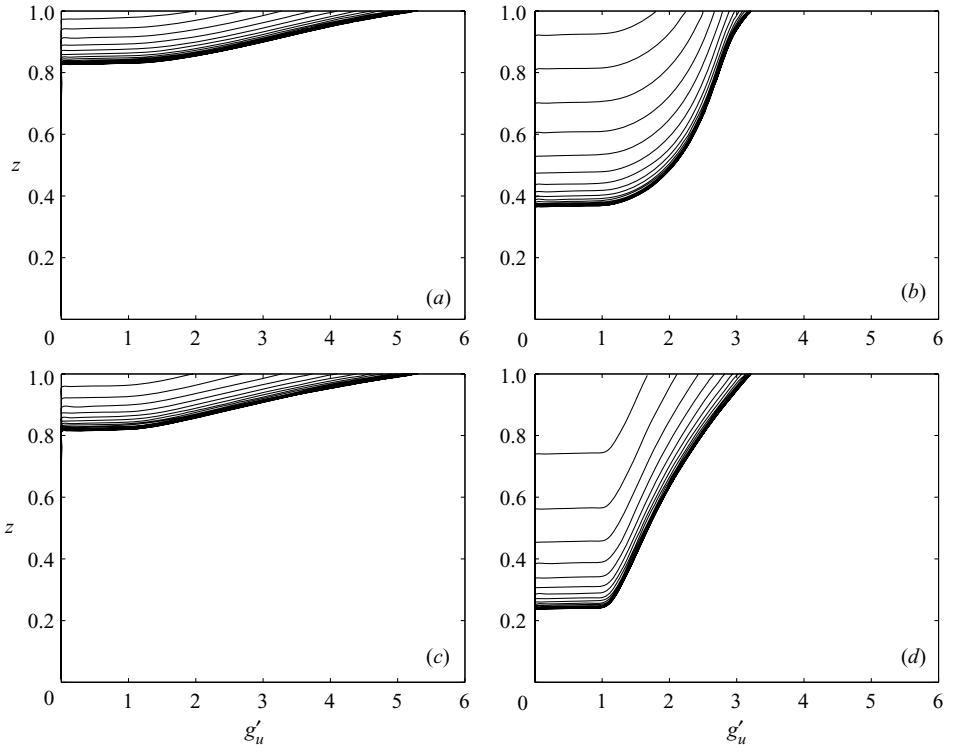

FIGURE 6. Profiles of $g'_u(z)$ predicted by the stratified S-S model at times $t = n/2$, $n = 1, 2, \ldots, 20$ for systems with $a_u = 1/2$, $h_l = 1/2$ and: (*a*) $a_t^2 = 0.1$, $a_b^2 = 0.1$; (*b*) $a_t^2 = 10$, $a_b^2 = 0.1$; (*c*) $a_t^2 = 0.1$, $a_b^2 = 10$; (*d*) $a_t^2 = 10$, $a_b^2 = 10$.

Indeed, large area openings connecting an unoccupied atrium to a forced chamber lead inevitably to extensive contamination of the unoccupied atrium. Our models predict that this behaviour occurs even when the exterior openings are designed to be of an adequate size for the buoyant layer in the forced chamber to be shallow, and the atrium has a relatively large cross-sectional area. This counter-intuitive behaviour appears to be due to the fact that the stratified buoyant layer in the unforced chamber is constituted of fluid from the buoyant layer in the forced chamber from different stages of the forced chamber's development. Subsequent use or occupation of the unforced chamber would then have to cope with this prior contamination by buoyant fluid from the forced chamber. For the buoyant fluid from the forced chamber to be flushed from the unforced chamber, it is essential for the openings to the exterior to be sufficiently large compared to the upper opening between the two chambers. This naturally involves a trade off, as such a design will inevitably lead to a deeper buoyant layer in the forced chamber. It thus appears sensible to avoid large disparity in the effective area $A_\star$ of the exterior openings and the upper interconnecting opening 't' to optimize the depth of each space which is not contaminated by buoyant fluid.

5. Laboratory experiments

To identify which of the numerical models we have discussed predicts better a real physical system, we have conducted a sequence of eight laboratory experiments. As is conventional, the experiments were conducted in an inverted geometry and used a

Experiment	h_l	a_p	a_u	h_v	$h_{f\infty}$	$h_{of\infty}$	$h_{su\infty}$	$h_{mu\infty}$	$h_{ou\infty}$
A	0.52	1	0.5	0.078	0.49	0.49	0.50	0.66	0.52
B	0.57	1	0.5	0.078	0.53	0.54	0.56	0.69	0.57
C	0.61	1	0.5	0.080	0.57	0.58	0.61	0.72	0.62
D	0.65	1	0.5	0.078	0.61	0.58	0.65	0.74	0.66
E	0.52	1	2	0.079	0.49	0.53	0.56	0.66	0.57
F	0.61	1	2	0.079	0.57	0.53	0.65	0.72	0.56
G	0.65	0.17	0.5	0.079	0.40	0.32	0.95	0.97	0.77
H	0.57	1.5	0.5	0.083	0.55	0.58	0.48	0.63	0.48

TABLE 1. Experimental parameter values.

descending saline plume. The experimental apparatus consisted of a Perspex tank of internal dimensions 91.6 cm × 30.5 cm × 31.1 cm. A thin internal partition divided the tank such that $a_u = \frac{1}{2}$ or $a_u = 2$. This internal partition contained a series of 2.54 cm diameter openings along its top and bottom. The chambers could also communicate with the external reservoir fluid through openings drilled along the tank's upper and lower surfaces. For simplicity, we considered circumstances where the external and internal partition openings were equal in size.

We chose $A_\star$ to vary from 6.08 cm^2 to 18.3 cm^2. The applicable non-dimensional parameters for the eight experiments are presented in table 1, where $a_t = a_b = a_p$. The chambers were suspended in a much larger reservoir (237.5 cm by 115.6 cm by 118.7 cm). This reservoir tank was filled to a depth of approximately 110 cm and the experimental tank was positioned such that its top surface was approximately 11 cm below the free interface. This top surface was fitted with a nozzle through which a saline solution was injected. The solution was itself fed from a constant pressure head overhead tank. Flow rates were controlled via a quarter-turn valve and measured using a rotameter. Red food colouring was added to the saline solution for the purposes of flow visualization.

For the experiments reported upon here, Q_s ranged from 1.8 to 1.9 cm^3 s^{-1}. B_s ranged from 80 cm^4 s^{-3} to 91 cm^4 s^{-3}. The nozzle design (due to Dr Paul Cooper, see Hunt & Linden 2001 for a more detailed discussion of the design) minimized the vertical adjustment length over which the flow became fully turbulent. We corrected for the 'effective origin' h_v (see Caulfield & Woods 1995), defined as

$$h_v \equiv \left(\frac{Q_s^2}{\lambda^3 G_s' H^5} \right)^{1/5}. \tag{5.1}$$

The effective origin h_v (also listed in table 1) defines the distance below the source over which a point-source plume, with the same buoyancy flux as the source, would have to rise to have the same volume flux as the source volume flux. We have verified that, due to the small value of the source volume flux, more sophisticated corrections (e.g. the asymptotic 'virtual origin' correction suggested by Hunt & Kaye 2001) or the results of a full calculation, considering the source volume flux and momentum flux explicitly, (as discussed in Woods *et al.* 2003 for the single chamber flow) lead to variations in predictions of interface height well within the range of experimental error.

Before a regular filling-box flow was established, a transient 'slumping' phase was encountered whereby the discharged plume fluid 'slosh[ed] up the sidewalls of the box' (Kaye & Hunt 2004) then subsequently collapsed into a layer of approximately uniform thickness (Hunt *et al.* 2001). Ambient fluid was entrained directly into this

contaminated layer. The initial density of this contaminated layer was smaller than that anticipated from the S-S model equations of § 3, which assume that a filling-box flow was established instantaneously. Whereas some fraction of this contaminated fluid was quickly re-entrained into the plume, the remaining portion was advected into the unforced chamber where it was either discharged through the external opening or accumulated in the expanding layer of dense fluid. Some non-trivial 'imprint' of this initial transient mixing was thus maintained in the unforced chamber, even in the long-time limit $t \to \infty$, which should lead to a divergence from the predictions of the stratified S-S model. Eventually a filling-box flow was observed, and the flow approached steady state on the expected time scale T_f.

We measured the steady-state interface locations in each chamber, which we determine using the 'maximum gradient' method of Kaye & Hunt (2004). In table 1, we list both the measured and the predicted steady-state locations for the interfaces in both the forced and unforced chamber for the eight different experiments. The predicted steady state of the interface in the forced chamber $h_{f\infty}$ can be compared with the equivalent value of h_l (defined in (2.7) for a single chamber flow) and the observed interface location (adjusted with the effective origin) $h_{of\infty}$.

As expected, the presence of the unforced chamber reduces the height of the interface above the source. This effect is most marked in the case of experiment 'G', when a_t is relatively small, and so the pressure loss through opening 't' is most significant, as $a_\dagger$ is dominated by a_t. In general, the S-S model accurately predicts the interface location in the forced chamber. The r.m.s. error between the observed measurements and the predictions of the S-S model is approximately 30 % of the r.m.s. error between the observed measurements and the predictions of the single chamber model, and so it appears possible to identify the effect of the unforced chamber quantitatively. (The well-mixed M-M model predicts the same interface location as the S-S model.)

In table 1, we also list the steady-state interface height in the unforced chamber predicted by the stratified S-S model $h_{su\infty}$, the interface height predicted by the well-mixed M-M model $h_{mu\infty}$, and the observed interface height (adjusted with the effective origin) $h_{ou\infty}$. In general, the stratified S-S model predicts the ultimate interface height much more accurately than the well-mixed M-M model, although for experiment 'G', both models significantly underestimate the observed depth of the buoyant layer in the unforced chamber. This mismatch occurs when the openings in the interconnecting partition are relatively small compared to the openings to the exterior, and the unforced chamber is relatively small compared to the forced chamber. The smaller interconnecting opening leads to a relatively high velocity through the opening 't' into the unforced chamber, and since the chamber has a small cross-sectional area, this relatively high velocity fluid is likely to lead to some overturning.

Nevertheless, the stratified S-S model is a much better predictor of the actual interface location, with the r.m.s. error between the experimental observations and the predictions of the S-S model being approximately 50% of the r.m.s. error between the experimental observations and the predictions of the well-mixed M-M model. The M-M model always predicts that the buoyant layer in the unforced chamber is shallower than the buoyant layer in the forced chamber, and the experimental evidence shows that this is an unjustified assumption. The evidence points strongly towards the requirement that, in general, the buoyant layer in the unforced chamber is stratified. For example, in experiment 'H', where the interconnecting openings were relatively large, the buoyant layer in the unforced chamber is both predicted by the S-S model and observed experimentally to be deeper than the buoyant layer in the forced chamber. Therefore, for the flow between interconnected chambers over a

wide range of parameter values, the buoyant layer depth in the unforced chamber is well-predicted by the full transient S-S model.

6. Conclusions

We have considered both the transient and steady-state flows which can develop in two interconnected chambers of the geometry shown in figure 1. The steady-state flow in the 'forced' chamber (containing an isolated point source of buoyancy flux) depends not only on the single chamber effective area $A_\star$ (defined in (2.4)), combining the lower exterior inflow opening 'i' in the forced chamber (with area A_i) and the upper exterior outflow opening in the unforced chamber (with area A_o), but also the top opening 't' in the interconnecting partition (with area A_t). The effect of the pressure drop associated with the flow through opening 't' is to reduce the apparent effective area of the openings to $A_\dagger \leqslant A_\star$ (and thus to increase the depth of the steady-state buoyant layer) compared to a single chamber flow with the same external openings, as considered in LLS90 (cf. (3.8) and (2.4)). Convergence towards this steady state occurs on the filling-box time scale T_f for the two chamber system as defined in (3.12).

Although the steady state in the forced chamber is well-mixed, and has no dependence on the previous time evolution of the flow, the steady state in the unforced chamber is typically stratified, and depends strongly on the time-dependent evolution of the flow towards its final steady state, as well as on the areas of all the openings and the cross-sectional areas of the two chambers. This is qualitatively different behaviour from that predicted by a model that assumes that the fluid in each chamber is always well-mixed. Such well-mixed models predict that the buoyant layer in the unforced chamber is always shallower than the buoyant layer in the forced chamber. However, evidence from analogue laboratory experiments supports the assumption that it is essential to track carefully the evolving stratification in the unforced chamber if the steady-state layer depth is to be predicted correctly, capturing well a situation where the unforced chamber's buoyant layer depth is actually deeper than the forced chamber's buoyant layer depth, which is well-predicted by a stratified model.

Of course, the flow considered here is extremely idealized. For example, we make the strong simplifying assumptions that the forced plume is a source of buoyancy alone, that the flow through the various openings is uni-directional for all time, and that the two chambers are initially filled with ambient fluid. Also, we assume that the openings are of infinitesimal vertical depth, which is clearly impossible for the interior openings. Therefore, there will inevitably be a pressure variation across the opening, and it is more appropriate to consider the pressure at the midpoint of the opening (see Hunt & Linden 2001 for a more detailed discussion). Indeed, it is much more likely that either exchange flows (as considered in Phillips & Woods 2004) or reversing flows (due perhaps to source volume flux associated with forced air heating or air conditioning systems, as discussed by Woods *et al.* 2003) may occur at different stages of the flow evolution, and that there is at least some buoyant fluid in either or both chambers initially.

Such contamination at the start of the flow evolution and variation in source conditions qualitatively modifies the ultimate steady state in the unforced room, due to complex interactions between the associated draining flows, blocking flows and filling-box flows associated with the plume in the forced chamber. In all probability, interactions of these kinds modify the paths connecting initial states to ultimate steady states. As a way to develop a more applicable understanding of real ventilation flows

in multi-chamber buildings, we aim to report on our analysis of the dynamical effects of these interactions in due course.

Financial support for M. R. F. was generously provided by NSERC (Canada), the Canadian Meteorological and Oceanographic Society and the University of California, San Diego through an Academic Senate Research grant. Engaging discussions with Professor Paul F. Linden, Dr Nigel B. Kaye and Mr Diogo Bolster are also acknowledged. Mr Thomas Chalfant provided invaluable assistance with equipment design and fabrication. Finally, the authors are very grateful for the insights of referees whose detailed comments have significantly improved the discussion.

Appendix A. Flow through opening 'b' for the S-S model

Considering the flows into the unforced chamber, if the flow remains stratified in the unforced chamber,

$$\frac{\mathrm{d}}{\mathrm{d}t}I_u = G'_f(H)(Q_t - Q_o) \qquad \text{if } Q_t \geqslant Q_o, \tag{A 1a}$$

$$= -G'_u(H)(Q_o - Q_t) \qquad \text{if } Q_t < Q_o, \tag{A 1b}$$

where $G'_f(H)$ and $G'_u(H)$ are the reduced gravities at the top of the forced and unforced chambers respectively. I_u increases if and only if $Q_b < 0$, and the depth of the buoyant layer in the unforced chamber increases. At least initially, $Q_t > Q_o$. Therefore, $Q_b < 0$, which implies that $P_u(0) > P_f(0)$, and so (3.9) applies. It is thus impossible for I_u to exceed $A_\dagger^2 I_f$, its steady-state value, and so as claimed in § 3.2, I_u approaches its steady-state value from below. If $I_u > A_\dagger^2 I_f$, $Q_t < Q_o$, and so I_u would have to decrease. This argument applies for all values of $I_u > A_\dagger^2 I_f$, thus implying that there is no possible time evolution by which I_u could grow transiently larger than $A_\dagger^2 I_f$ while still being required to approach this value at steady state.

Appendix B. Flow through opening 'b' for the M-M model

If the flow is assumed to be well-mixed in the unforced chamber, the appropriate equation for the evolution of the buoyancy integral I_u becomes

$$\frac{\mathrm{d}}{\mathrm{d}t}I_u = G'_f(H)Q_t - G'_u Q_o, \tag{B 1}$$

where $G'_f(H)$ is the reduced gravity at the top of the forced chamber, and G'_u is the (well-mixed) reduced gravity of the unforced chamber. Provided $G'_f(H)$ is sufficiently large compared to G'_u, it is entirely possible for I_u to increase when $Q_t < Q_o$, at least initially, and hence the argument presented in Appendix A does not apply. Therefore, it is possible for the buoyancy integral I_u to be sufficiently large for the pressure $P_f(0)$ in the forced chamber at $Z = 0$ to be greater than the pressure $P_u(0)$ in the unforced chamber at $Z = 0$, and so the flow Q_b through opening 'b' is positive (i.e. from the forced to the unforced chamber) and is given by

$$Q_b = A_b\left(\frac{2}{\rho_e}[P_f(0) - P_u(0)]\right)^{1/2} = A_b\left[\frac{Q_t^2}{A_t^2} - 2(I_f - I_u)\right]^{1/2}, \tag{B 2}$$

using (3.2). Using this expression, rather than (3.9), the system is now closed, and using the same non-dimensionalization and approach as in the main body of the text, the flow q_o must satisfy

$$q_o^2 = \frac{i_u}{\mu^2} + \frac{\left[1+2\left(a_t^2-a_b^2\right)\right]\left[1+2a_t^2\right]\left[a_\dagger^2 i_f - i_u\right] - 4a_b^2 i_u}{\mu^2\left[1+4\left(a_b^2+a_t^2\right)+4\left(a_b^2-a_t^2\right)^2\right]} + \frac{\left[16a_b^4 i_u^2 + 16a_b^2\left(1+2a_t^2\right)\left(a_\dagger^2 i_f - i_u\right)\left(a_b^2 i_u - a_t^2 i_f\right)\right]^{1/2}}{\mu^2\left[1+4\left(a_b^2+a_t^2\right)+4\left(a_b^2-a_t^2\right)^2\right]}. \quad \text{(B 3)}$$

All the other volume fluxes can be determined from (3.15). Using (B 2), it is possible to establish that the requirement that $q_o > q_t$ implies that

$$i_u \geqslant \mu^2 q_o^2 \geqslant a_\dagger^2 i_f, \quad \text{(B 4)}$$

and so $a_\dagger^2 i_f - i_u \leqslant 0$ in this circumstance.

REFERENCES

Baines, W. D. & Turner, J. S. 1969 Turbulent buoyant convection from a source in a confined region. *J. Fluid Mech.* **37**, 51–80.

Caulfield, C.-C. P. & Woods, A. W. 1995 Plumes with nonmonotonic mixing behaviour. *Geophys. Astrophys. Fluid Dyn.* **79**, 173–199.

Caulfield, C. P. & Woods, A. W. 2002 The mixing in a room by a localized finite-mass-flux source of buoyancy. *J. Fluid Mech.* **471**, 33–50.

Conroy, D. T., Llewellyn Smith, S. G. & Caulfield, C. P. 2005 Evolution of a chemically reacting plume in a ventilated room. *J. Fluid Mech.* **537**, 221–253.

Germeles, A. E. 1975 Forced plumes and mixing of liquids in tanks. *J. Fluid Mech.* **71**, 601–623.

Gladstone, C. & Woods, A. W. 2001 On buoyancy-driven natural ventilation of a room with a heated floor. *J. Fluid Mech.* **441**, 293–314.

Hunt, G. R., Cooper, P. & Linden, P. F. 2001 Thermal stratification produced by plumes and jets in enclosed spaces. *Building Environ.* **36**, 871–882.

Hunt, G. R. & Kaye, N. G. 2001 Virtual origin correction of lazy turbulent plumes. *J. Fluid Mech.* **435**, 377–396.

Hunt, G. R. & Linden, P. F. 2001 Steady-state flows in an enclosure ventilated by buoyancy forces assisted by wind. *J. Fluid Mech.* **426**, 355–386.

Kaye, N. B. & Hunt, G. R. 2004 Time-dependent flows in an emptying filling box. *J. Fluid Mech.* **520**, 135–156.

Lin, Y. J. P. & Linden, P. F. 2002 Buoyancy-driven ventilation between two chambers. *J. Fluid Mech.* **463**, 293–312.

Linden, P. F. 1999 The fluid mechanics of natural ventilation. *Annu. Rev. Fluid Mech.* **31**, 201–238.

Linden, P. F., Lane-Serff, G. F. & Smeed, D. A. 1990 Emptying filling boxes: the fluid mechanics of natural ventilation. *J. Fluid Mech.* **212**, 309–335 (referred to herein as LLS90).

List, E. J. 1982 Turbulent jets and plumes. *Annu. Rev. Fluid Mech.* **14**, 189–212.

Manins, P. C. 1979 Turbulent buoyant convection from a source in a confined region. *J. Fluid Mech.* **91**, 765–781.

Morton, B. R., Taylor, G. I. & Turner, J. S. 1956 Turbulent gravitational convection from maintained and instantaneous sources. *Proc. R. Soc. Lond.* A **234**, 1–23.

Phillips, J. C. & Woods, A. W. 2004 On ventilation through a single doorway. *Building Environ.* **39**, 241–253.

Turner, J. S. 1969 Buoyant plumes and thermals. *Annu. Rev. Fluid Mech.* **1**, 29–44.

Woods, A. W., Caulfield, C. P. & Phillips, J. C. 2003 Blocked natural ventilation: the effect of a source mass flux. *J. Fluid Mech.* **495**, 119–133.

Wong, A. B. D. & Griffiths R. W. 2001 Two-basin filling boxes. *J. Geophys. Res.* **C106**, 26929–26941.

Worster, M. G. & Huppert, H. E. 1983 Time-dependent density profiles in a filling box. *J. Fluid Mech.* **132**, 457–466.

Zeldovich, Y. B. 1937 The asymptotic laws of freely-ascending convective flows. *Zhur. Eksper. Teor. Fiz.* **7**, 1463–1465 (in Russian). English transl. in *Selected works of Yakov Borisovich Zeldovich*, Vol. 1 1992 (ed. J. P. Ostriker), pp. 82–85. Princeton University Press.